Interaction of Engineered Nanoparticles with Artificial Cell Membranes

Rachel Benton

Chemical Engineering, North Carolina State University

NNIN REU Site: NanoTech User Facility, University of Washington, Seattle, WA
NNIN REU Principal Investigator: Jonathan D. Posner, Mechanical and Chemical Engineering, University of Washington
NNIN REU Mentor: Charles Corredor, Chemical Engineering, University of Washington
Contact: rabento2@ncsu.edu, jposner@uw.edu, corredor@uw.edu

Abstract:

Understanding the potential toxicity of engineered nanoparticles (ENPs) is vital due to their presence in over 1300 commercial products (e.g. toothpaste, sunscreen, and anti-bacterial coating on blankets). To further evaluate the potential consequences of ENPs, research must be performed to examine the interaction and mechanistic behavior between these particles and biological systems. This study seeks to understand these interactions by characterizing the effects of ENPs on artificial cell membranes. Understanding the interaction of engineered nanoparticles with lipid bilayers is an important step toward predicting subsequent biological effects and facilitates the design of safe nanoproducts. We believe that under some conditions ENPs can passively translocate across, and cause nanoscale defects in, lipid membranes. In this work, we quantify the disruption of liposomes induced by ENPs using a dye leakage assay. We measure dye leakage from lipid vesicles loaded with carboxy-fluorescein dye that are exposed to a diverse selection of ENPs. The amount of dye released correlated directly to the level of interaction between nanoparticles and the lipid vesicles.

Introduction:

Engineered nanoparticles (ENPs) are being utilized in various commercial ventures and research studies. Because of the rapid growth in the field of nanotechnology, there is a high potential that at some point in these particles' lifespan, they will come in to contact with the environment and humans [1, 2]. As of yet, the effects of these particles on health and the environment are not sufficiently well known. While ENPs hold a great deal of promise, before reaping the benefits of nanotechnology, more extensive research must be done in the field of nanotoxicity to understand their potential risks.

Membrane permeability is a vital component of toxicity studies as the membrane controls what enters and exits a cell. Lipid bilayers serve as viable artificial cell membranes in that natural cell membranes are comprised of over 80% lipids [3]. These same lipids, due to their hydrophilic head and hydrophobic tail, will self-assemble into spherical liposomes. This study seeks to understand the interaction of nanoparticles with artificial cell membranes by characterizing the effects of ENPs on liposome permeability using a dye leakage assay of liposomes exposed to ENPs.

Preparation:

Phospholipids were suspended in carboxyfluorescein (fluorescent dye), forming lipid bilayers, then passed through a 100 nm polycarbonate membrane in the process of extrusion. This caused a homogenous population of liposomes to form. As the liposomes formed, they encapsulated carboxyfluorescein inside them. The resulting solution was washed using unltracentrifugation by forcing it through a 3kDa membrane to remove the excess dye from outside the liposomes. This left just the liposomes (diameter approximately 100 nm) loaded with carboxyfluorescein.

This liposome, with the entrapped fluorescent dye, was then exposed to target ENPs. These experiments focused on two types of silver (Ag) ENPs, each with a 20 nm core diameter; one coated with polyvinylpyrrolidone (PVP), and the other with sodium citrate (NaCT). If the nanoparticles caused a disruption in the lipid bilayer, then the dye encapsulated inside the liposome would leak out. This amount of leakage was measured using fluorescent spectroscopy.

The carboxyfluorescein was excited at 480 nm and emitted at 520 nm. Because of this, the intensity measurements from the spectrometer were taken at 517.5 nm. The percent of leaked dye was found using the following formula:

$$Percent\ Leakage = \frac{I - I_{min}}{I_{max} - I_{min}} \times 100$$

where I is the intensity after liposomes are exposed to ENPs, I_{min} is the intensity of the liposomes without any ENP exposure, and I_{max} is the intensity after the liposomes are treated with Triton-X, which is known to cause total leakage from the nanoparticles.

The percent leakage was measured for three different conditions: liposomes without nanoparticle exposure, liposomes exposed to Ag NPs coated with PVP, and liposomes exposed to Ag NPs coated with NaCT.

Results:

Figure 1 and 2 show the percent leakage induced by Ag NPs as a function of time for 112 and 5600 PPB, respectively. The average percent leakage of fluorescent dye from the liposomes exposed to Ag NPs for both coatings was consistently higher than the liposomes without exposure for all tests. This showed a clear interaction between the ENPs and liposomes. In Figure 2, at approximately 1500 minutes, a greater percent leakage for liposomes exposed to sodium citrate coated Ag NPs was evident. The leakage also increased with increasing concentration. These results suggest that the surface functionality is a critical parameter in governing the disruption of bilayers induced by ENPs.

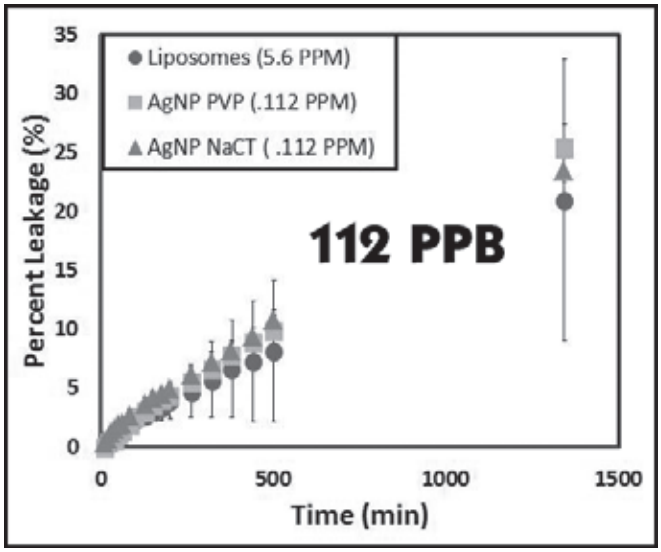

Figure 1: Kinetic measurements of liposomes after exposure to Ag NPs.

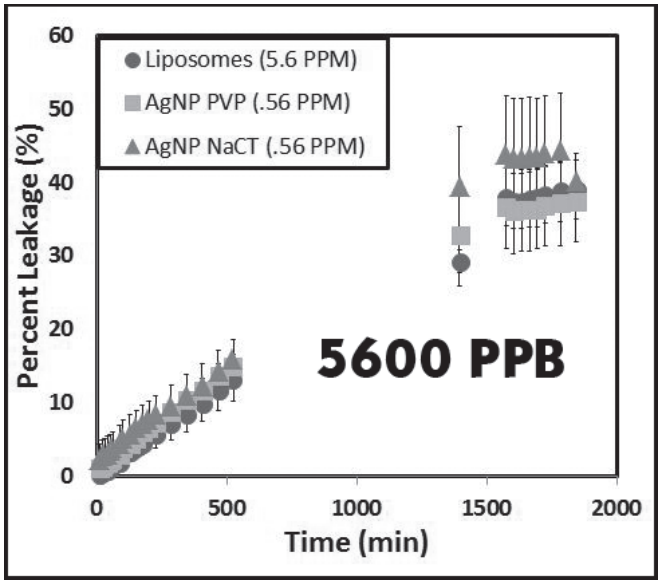

Figure 2: Kinetic measurements of liposomes after exposure to Ag NPs.

Summary:

These results show that ENPs disrupt bilayers and induce leakage of their internal contents. However, it cannot be inferred from this experiment whether or not these ENPs are toxic. Showing an interaction between ENPs and liposomes is an evidence that these ENPs are causing a disruption in the lipid bilayer and thus potentially in cell membranes, but the biomechanics of this interaction remain unknown. Understanding the interaction of ENPs with lipid bilayers is an important step toward predicting subsequent biological effects and facilitates the design of safe nanoproducts.

Acknowledgements:

I thank my Principal Investigator, Dr. Posner, and my mentor, Charles Corredor, as well as the rest of the Posner Research Group. I also acknowledge the National Science Foundation and the National Nanotechnology Infrastructure Network Research Experience for Undergraduates Program for the funding of my research. Thank you to University of Washington's Nanotech User Facility and to my program coordinator, Mack Carter. Finally, I would like to acknowledge Dr. Smith and Dr. Kavanagh from the Nanotoxicology Center at University of Washington with whom we collaborated with on this project.

References:

[1] Dean, L. Measurement helps solve nanoparticle toxicity challenges. Chemistry International, 34(4) (2012, July).

[2] Nel, A. E., Madler, L., and Velegol, D. Understanding the biophysicochemical interactions at the nano-bio interface. Nature. (2009).

[3] Roiter, Y., Ornatska, M., and Aravind, R. R. Interaction of nanoparticles with lipid membrane. Nano Letters, 8(3), 941-944. (2008).

Fabricating Parylene-C Shadow Masks for Applications in Short-Channel Top-Contact Carbon Nanotube Flexible Transistors

Kelsey Hirotsu

Chemical and Biomolecular Engineering, Johns Hopkins University

NNIN REU Site: Stanford Nanofabrication Facility, Stanford University, Stanford, CA
NNIN REU Principal Investigator: Professor Zhenan Bao, Chemical Engineering, Stanford University
NNIN REU Mentor: Evan Wang, Materials Science and Engineering, Stanford University
Contact: khirotsu@jhu.edu, zbao@stanford.edu, whl0903@stanford.edu

Abstract:

Flexible transistors with semiconducting carbon nanotubes offer better mobility and stability than current organic material transistors for applications in flexible display and sensor devices. With carbon nanotubes as the semiconducting material, the transistors offer a higher performance due to the extraordinary electrical properties of single-walled carbon nanotubes (SWNTs). However, conventional metal shadow masks can only create flexible device transistors with a channel length of 50 μm or greater. Parylene-C shadow masks can be used instead of metal masks because of their flexibility, adaptability for patterning, and their ability to fabricate transistors with much smaller channel lengths. Previously it has been shown that Parylene-C masks allow for a fine resolution with a smallest feature size of 4 μm. We fabricated masks with features as small as 2 μm wide, and additionally used our masks to create short-channel transistors. We successfully constructed short-channel top-contact SWNT network inflexible and flexible transistors on silicon (Si) and polyamide substrates with a mobility of 0.1 to 2 cm^2/V-s and on/off ratios on the magnitude of 10^2 to 10^3.

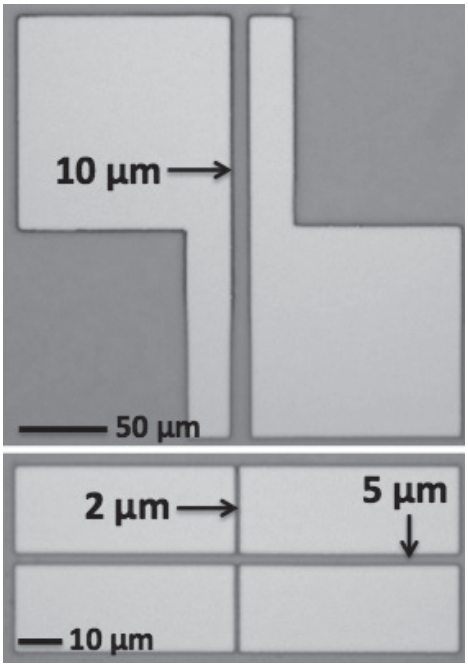

Figure 1: 2, 5, and 10 µm features etched into parylene on Si substrate.

Introduction:

Parylene-C is a polymer that is flexible, transparent, biocompatible, and relatively inexpensive. Its characteristics allow for Parylene-C shadow masks to have the potential for various micropatterning applications [1]. Unlike conventional hard masks, parylene masks adhere to the surface of the substrate for better contact between the substrate and the stencil. While conventional hard masks can create features as small as 50 μm wide, parylene masks have been used to make features as small as 4 μm wide. Previously, flexible transistors have been fabricated with semiconducting carbon nanotube networks [2]. Short-channel inflexible transistors have also been fabricated, using Parylene-C shadow masks [3]. To optimize the performance of our flexible transistors, we combined features of both previously fabricated devices. We aimed to make Parylene-C shadow masks for use in the fabrication of short-channel flexible transistors with solution-sorted semiconducting carbon nanotube networks.

Experimental Procedure:

To fabricate the parylene masks, we adopted a previously developed procedure to fit the capabilities of the Stanford Nanofabrication Facility and Bao lab equipment [1]. We exposed 4-inch silicon wafers coated with 15 μm of parylene to oxygen plasma at 150 W RF power and at 150 mTorr to roughen the parylene to enhance aluminum adhesion. Then we evaporated 200 nm of aluminum onto the parylene and created a hard mask through conventional optical lithography. We patterned the aluminum through a wet etch (72% phosphoric acid, 3% nitric acid, 3% acetic acid, 22% water). Then we etched the parylene with oxygen plasma for one hour at the same parameters previously used to roughen the parylene, and finally, we etched away the aluminum hard mask with the same wet etchant (Figure 1).

To fabricate transistors with the parylene mask, we prepared substrate samples by soaking them in purified semiconducting SWNT solutions. To purify semiconducting SWNTs from metallic SWNTs, we used the Bao group's previously developed sorting process [4]. We peeled the mask off of the silicon wafer and placed it on the new substrate with carbon nanotubes, and then evaporated 40 nm of gold over the mask to fabricate the transistors (Figure 2 and 3).

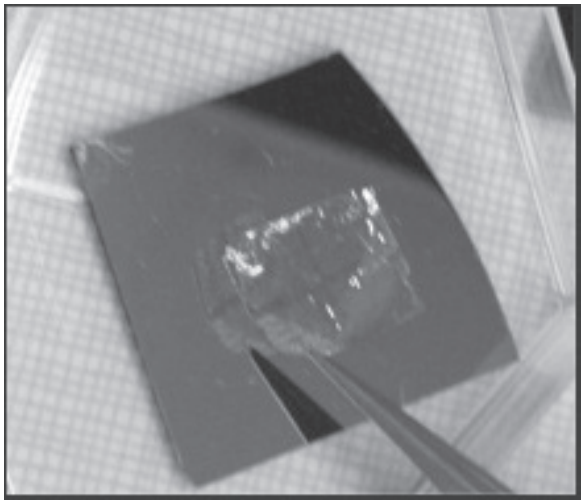

Figure 2: Parylene mask peeled off of Si substrate.

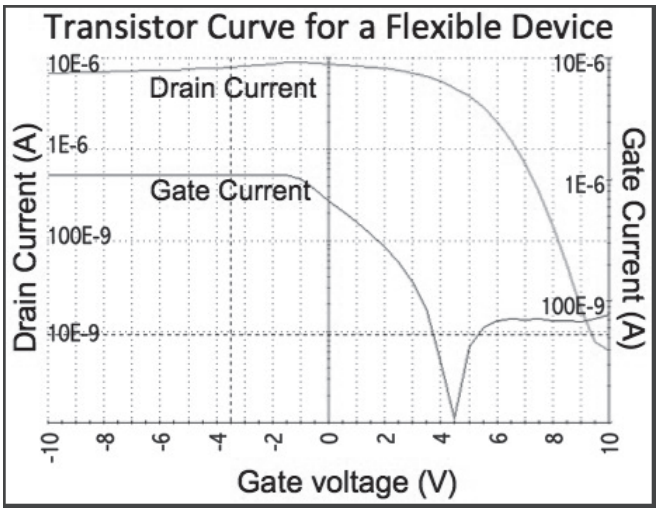

Figure 4: Keithley-generated flexible transistor curve.

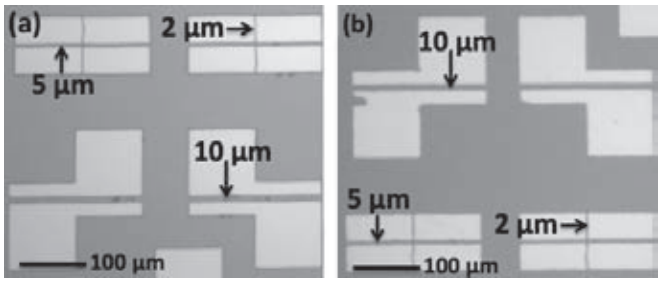

Figure 3: (a) Parylene mask placed onto SWNT-soaked substrate; (b) Gold on SWNT-soaked substrate after mask removal.

After the gold evaporation, we peeled the mask off and tested the transistors for their performance.

Results and Discussion:

We consistently fabricated Parylene-C shadow masks with etched features ranging from 2 μm to 50 μm wide. The process was optimized and scaled-up to full wafer scale production of shadow masks. We fabricated inflexible and flexible transistors with the parylene masks and then tested the performance by measuring the current flow across transistors at various applied gate voltages. Both types of devices had a mobility of 0.1 to 2 cm^2/V-s and on/off ratios on the magnitude of 10^2 to 10^3 for channel widths of 20 μm (Figure 4).

Although we fabricated transistors as small as 2 μm wide, it was difficult to test these transistors with the equipment we had. Therefore we only tested features 5, 10, 20 and 30 μm wide. From testing the inflexible and flexible transistors, the data indicated that we had fabricated functioning devices with good on/off ratios and mobilities. Furthermore, the parylene masks allowed for consistent transistor fabrication within a sample and between samples as well. The on/off ratios and mobility results for flexible transistors were similar to that of inflexible transistors, indicating that the flexible substrate did not hinder the performance of the device.

Future Work:

We aim to continue fabricating short-channel top-contact carbon nanotube flexible transistors to optimize their performance. Furthermore, bending tests will be conducted on the flexible transistors to assess their performance during and after strain. We also aim to optimize the purification process of the semiconducting carbon nanotubes using various solvents and polymers.

Acknowledgements:

I would like to thank Professor Zhenan Bao, my mentor Evan Wang, the Bao Group at Stanford, Site Coordinator Michael Deal, Maureen Baran, the Stanford Nanofabrication Facility staff, the NNIN REU Program Coordinators, and lastly the NNIN, NSF, and CIS for financial support.

References:

[1] S. Selvarasah; "A reusable high aspect ratio Parylene-C shadow mask technology for diverse micropatterning applications"; ScienceDirect, vol 145-146, pp 306-315 (2008).

[2] C. Wang; "Extremely bendable, high-performance integrated circuits using semiconducting carbon nanotube networks for digital, analog, and radio-frequency applications"; Nano Letters, vol 12, pp 1527-1533. (2012).

[3] Y. Chung; "Low-voltage and short-channel pentacene field-effect transistors with top-contact geometry using Parylene-C shadow masks". Applied Physics Letters, vol 96 (2010).

[4] H.W. Lee; "Selective dispersion of high purity semiconducting single-walled carbon nanotubes with regioregular poly(3-alkylthiophene)s"; Nature Communications, vol 2 (2011).

The Electrochemistry of Catalyzed Metal Multilayers

Briana James
Engineering Science, University of Virginia

NNIN REU Site: Howard Nanoscale Science and Engineering Facility, Howard University, Washington, DC
NNIN REU Principal Investigator and Mentor: Dr. Tina Brower-Thomas, Chemical Engineering, Howard University
Contacts: bnj3dw@virginia.edu, tina.browerthomas@howard.edu

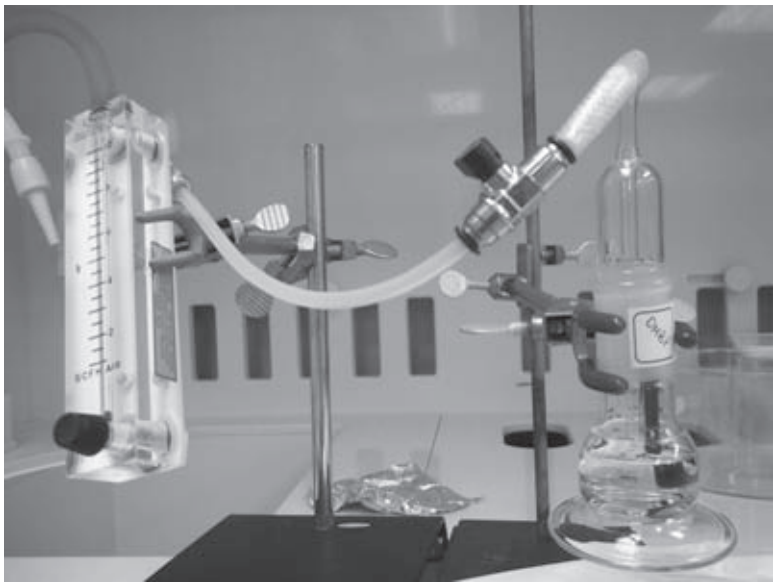

Figure 1: Research setup.

Abstract:

Self-assembled multilayers (SAM) are a product of the bottom-up fabrication method, a technique in which substances are built from the molecular level through chemical reactions. With thoughtful manipulation, such fabrications could perform as numerous components in molecular devices. This project utilized the bottom-up method to produce multilayers of the 4,'4 dimercaptobiphenyl (DMBP) attached to the group (II) B metal mercury (Hg). The focus was to analyze its electrochemical properties by cyclic voltammetry to determine if the structure could successfully conduct electrons. A current of potential energy was ramped up and inverted through the sample and the oxidation state of the mercury was analyzed. This reading concluded if mercury was being reduced. Currently a peak occurred around the potential 0.4 V when a monolayer of DMBP was capped with mercury, but the peak did not occur when bonded with a second DMBP. Trials are being conducted for confirmation of current data, to determine if multiple oxidation states of mercury are present, and provide understanding of other chemical properties of the substance.

Preparation of Multilayers:

The initial monolayer was prepared by introducing a gold working electrode to a 1 μM DMBP solution with 200 proof ethanol. The gold working electrode, with a disk diameter of 1.6 mm, was placed into the monolayer solution in a nitrogen atmosphere for three hours, as seen in the setup in Figure 1. The electrode was then rinsed off with ethanol and dried with a nitrogen jet gun. Mercury was introduced to the monolayer via a dilute solution of 0.008M mercury perchlorate ($Hg(ClO_4)_2 \cdot (6H_2O)$) and 200 proof ethanol. The electrode was again positioned in the solution for three hours with nitrogen, thoroughly washed with distilled water and ethanol, and then dried off with nitrogen. The gold electrode was alternatively introduced to the monolayer and mercury solution, creating DMBP and mercury multilayer. A cartoon of the assembled structure is shown in Figure 2. After every layer, cyclic voltammetry was performed to measure the sample's electrochemistry.

Cyclic Voltammetry:

Cyclic voltammetry determines the electrochemical properties of a sample through a series of cathodic and anodic measurements. For this experiment, our general setup included three electrodes enclosed in a glass cell partially filled with a 0.1 M sodium perchlorate electrolyte solution. The gold electrode served as the substrate for the various monolayers formed. Its potential energy was ramped up to a maximum current of 600 mV, then inverted to a set minimum of -600 mV, scanning the sample for two sweeps and six sweeps. The known electrochemical behavior of the silver/silver chloride electrode was used as a reference to measure the potential energy of the working electrode. A platinum counter electrode maintained a stable environment for oxidation and reduction.

Results:

Two attempts were completed. In the first attempt, five layers were made, three being the DMBP monolayer and two being Hg. Cyclic voltammetry of the first layer showed few peaks,

however as we continued building layers, a gradual increase in cathodic and anodic peaks occurred. Unfortunately, in the first attempt, we failed to eliminate oxygen as a factor in the experiment. We noticed this because of some peaks that were present that we could not attribute solely to the expected chemical reaction. We alleviated this problem in our second attempt by degassing the entire cell for 10 minutes prior to measuring the electrochemistry of the sample. During the second trial, we grew a total of three layers, two DMBP monolayers amid one layer of Hg. The sample with just the DMBP layer had very little peaks, similar to the results in the previous trial. The trial pertaining to the DMBP monolayer capped with a layer of Hg had two cathodic peaks, appearing around potential values of 500 mV and -200 mV. The same sample also had one anodic peak at an approximate potential value of -130 mV. Once another layer of DMBP was assembled on top of the DMBP and Hg layers, the cyclic voltammetry showed similar occurrences of very little peaks. Graphs of both attempts are depicted in Figure 1 and Figure 3.

Conclusions:

The occurrence of the anodic and cathodic peaks discussed previously indicates a significant change in the chemical behavior of the sample, suggesting successful formations of the DMBP and Hg multilayers. The sample capped with DMBP showed very few peaks, correlating with our expectations. At this state, Hg is not exposed to the electrolyte solution and there is no free electron available to react with the Hg. Future works would include continuing further trials on DMBP and Hg multilayers, and replacing DMBP with other organic molecules.

Acknowledgements

I would like to offer my deepest gratitude to: Dr. Tina Brower-Thomas, Dr. Charles Hosten, Dr. Yilma Gultneh, Mr. Maraizu Ukaegletgobu, Ms. Heather Battiste-Alleyne, Mr. James Griffin, and the staff of HNF, the National Nanotechnology Infrastructure Network Research Experience for Undergraduates (NNIN REU) Program, and the National Science Foundation (NSF).

References:

[1] Brower, T. "Self-Assembled Multilayers of 4,4'-Dimercaptobiphenyl Formed by Cu(II)-Catalyzed Oxidation"; Langmuir, 18, 6207-6216, (2002).

[2] Brower, T. "Growth of 4,4'-Dimercaptobiphenyl Using Group (II) B Elements"; Howard University Department of Chemical Engineering.

Figure 2: Multilayers of DMBP and Hg on gold substrate.

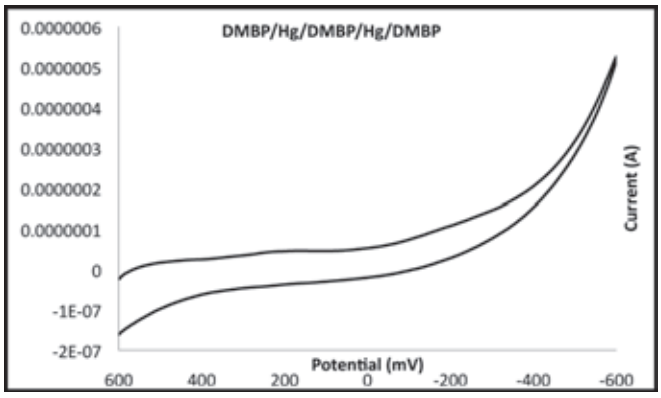

Figure 3: Cyclic voltammetry of first attempt with three DMBP monolayers and two layers of Hg.

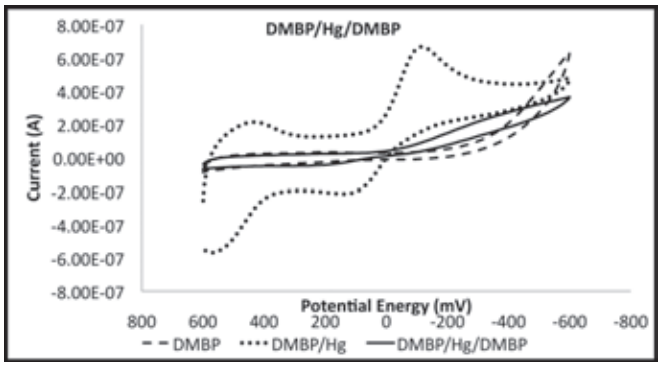

Figure 4: Cyclic voltammetry of second attempt with two DMBP monolayers amid a layer of Hg.

Implementing Gaussian Quadrature in Molecular Plasmonics

Alexander B. Lee

Mathematical and Computational Biology, Harvey Mudd College

NNIN REU Site: NanoTech User Facility, University of Washington, Seattle, WA
NNIN REU Principal Investigator: Professor David J. Masiello, Department of Chemistry, University of Washington
NNIN REU Mentor: Jonathan P. Litz, Department of Chemistry, University of Washington
Contact: ablee@hmc.edu, masiello@uw.edu, jlitz@gmail.com

Abstract:

For certain metals that support localized surface plasmon resonances, the resonant frequency of the material's electrons falls within the realm of visible light. We can use light to collectively and coherently oscillate the surface electrons in nanoparticles made up of these metals, magnifying the light in intensity. Such an environment could potentially be used to catalyze reactions occurring near these particles. Interactions between the molecules and the nanoparticle may alter the molecular electronic landscape into a configuration that is favorable to the reaction. This interaction occurs in part through the image effect. The goal of this project was to develop a computationally feasible process in which to determine the molecule's electronic structure after it has been image-dressed by a nanoparticle of arbitrary shape. In order to make larger molecules more tractable, we implemented Gaussian quadrature instead of the trapezoidal rule to calculate the contour integral describing the electron density of the molecule. This change resulted in the code running approximately 100 times faster than before.

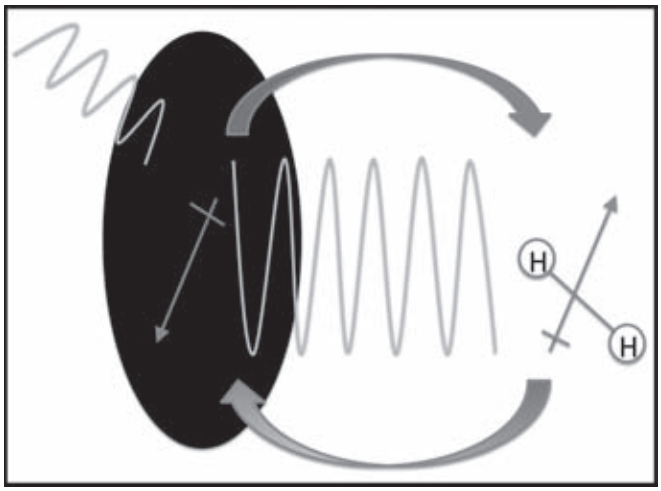

Figure 1: The molecule and nanoparticle repeatedly perturb each other through the image effect.

Introduction:

When a localized surface plasmon resonance (LSPR)-supporting metal nanoparticle is excited with light, its surface electrons oscillate collectively and coherently. When multiple LSPR nanoparticles are brought together, hot spots form, localized regions of high electric field intensity. These hot spots could be used in catalytic applications [1, 2]. Subjecting the molecules to these electric fields will alter the electronic landscape of the molecules into something that is hopefully more favorable for the desired reaction.

The nanoparticle and the molecule interact through the image effect [3, 4]. The electric field from the plasmon pushes the electrons in the molecule, inducing a dipole moment. This dipole gives off its own electric field, pushing the electrons in the nanoparticle into an "image" dipole, thus reducing the net electric field inside the metal to zero. However, rearranging the electrons affects the plasmon, altering the resulting electric field. This altered electric field induces a new dipole in the molecule (see Figure 1). In this way, the nanoparticle and the molecule interact with each other an infinite number of times until the system converges to some configuration.

It was the goal of this project to develop a computationally feasible process to determine the electronic structure of this image-dressed molecule.

Methodology:

We started by calculating the interacting Green's function, $\mathcal{G}$, for a molecule interacting with a nanoparticle [4]. We can use the Dyson expansion to write $\mathcal{G}$ as an infinite geometric series as shown in Figure 2, where G is the noninteracting Green's function for the molecule in vacuum and Σ is the self-energy [5]. Σ takes into account a single perturbation experienced by the molecule. Thus by calculating this infinite series, we took into account the infinite number of perturbations experienced by the molecule.

$$\mathcal{G} = G + (\Sigma G)G + (\Sigma G)^2 G + (\Sigma G)^3 G + \ldots$$

Figure 2: The Dyson expansion of the interacting Green's function.

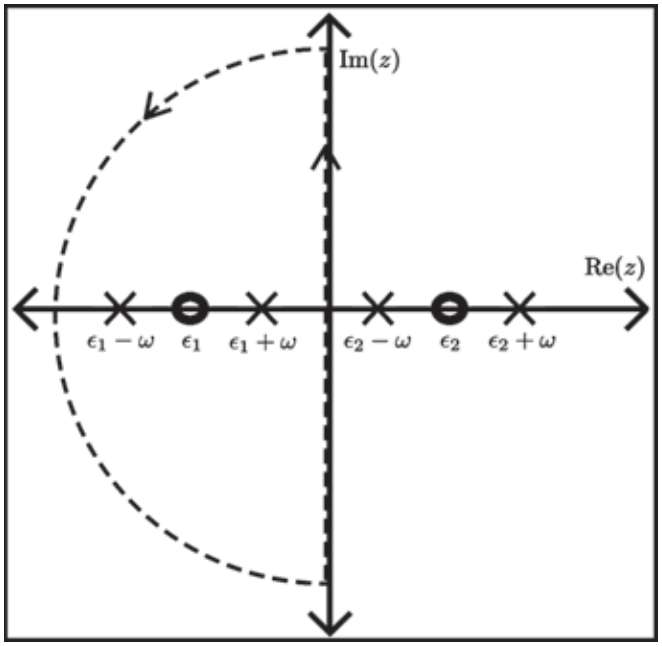

Figure 3: $\mathcal{G}$ is integrated around singularities associated with occupied orbitals to obtain the interacting one-matrix.

We then took the integral of $\mathcal{G}$ with respect to z, the frequency of interaction between the nanoparticle and the molecule. We integrated along a contour that encapsulated all singularities associated with occupied orbitals (see Figure 3). By computing this contour integral, we obtained the interacting one-matrix [6, 7]. Thus we were able to gain information on the electronic structure of the molecule in the form of an electron density.

To increase the speed of the code, Gaussian quadrature was implemented to numerically calculate the contour integral. Gaussian quadrature approximates the function as a 2n-1 degree Taylor polynomial, where n is the number of points taken. It does this by intelligently sampling the function as seen in Figure 4, where the x_i's are the locations at which the function is sampled, and the w_i's are the corresponding weights. These values are calculated independently from the function by a nonlinear system of 2n equations.

By switching from the trapezoidal rule to Gaussian quadrature, we reduced the number of times we needed to sample the function from 100,000 to 1000. Thus, this change made the code approximately 100 times faster than before. This made larger molecules, such as azulene, become more tractable as input molecules.

$$\int_{-1}^{1} f(x)dx \approx \sum_{i=1}^{n} w_i f(x_i)$$

Figure 4: Gaussian quadrature intelligently samples the function in order to approximate the integral.

Future Work:

In its current state, the code only performs calculations for the alteration of one electron. We hope to further develop this process to consider the configuration of all electrons at the same time. This will allow us to make predictions in experimental spectroscopies as well as begin to model catalytic applications of plasmonics.

Acknowledgements:

I would like to thank the National Nanotechnology Infrastructure Network Research Experience for Undergraduates (NNIN REU) Program, the National Science Foundation and the University of Washington, with special thanks to my principal investigator, Professor David J. Masiello, my mentor, Jonathan P. Litz, and my site coordinator, Mack Carter.

References:

[1] Christopher, P., H. Xin, and S. Linic, Nat. Chem. 3, 467 (2011).

[2] Liu, Z., W. Hou, P. Pavaskar, M. Aykol, and S. B. Cronin, Nano Lett. 11, 1111 (2011).

[3] Masiello, J. D. and G. C. Schatz, Phys. Rev. A 78, 064102 (2008).

[4] Masiello, J. D. and G. C. Schatz, J. Chem. Phys. 132, 064102 (2010).

[5] Fetter, A. L. and J. D. Walecka, "Quantum theory of many-particle systems," Chap. 3, (Dover ed, 2003).

[6] Holleboom, L., and J. Snijders, Int. J. Quantum Chem. 34 289 (1988).

[7] Holleboom, L., and J. Snijders, Int. J. Quantum Chem. 43, 259 (1992).

[8] Litz, J., R. Brewster, A. Lee, and D. Masiello, in preparation (2012).

Identification of Carbon Nanostructures (Fullerenes) in Cigarette Ash

Ian MacKenzie
Chemistry, Geneva College

NNIN REU Site: Nano Research Facility, Washington University in St. Louis, St. Louis, MO
NNIN REU Principal Investigator and Mentor: Dr. John Fortner, Department of Energy, Environmental and Chemical Engineering, Washington University in St. Louis
Contact: ian.mackenzie@geneva.edu, jfortner@seas.wustl.edu

Abstract:

The production of fullerene materials (C_{60}, C_{70}, etc.) has recently become a matter of increasing commercial interest and environmental concern. Although fullerene toxicity remains poorly defined, some forms have been shown to have cytotoxic effects, particularly when exposed to microbial communities. Therefore, the identification of (potential) fullerene sources is an important first step towards an accurate environmental exposure assessment. In this work, we tested the hypothesis that fullerenes (as C_{60} and C_{70}) are formed in burning cigarettes by analyzing ash from several scenarios, including mimicked smoking events.

Introduction:

Since the discovery of fullerene in 1985 by Kroto, et al., many synthetic methods have been proposed. Of particular interest is the synthesis of fullerene via pyrolysis of naphthalene [1]. This low molecular weight polycyclic aromatic hydrocarbon (PAH) can be found in environmentally significant quantities in coal tar, hydrocarbon fuels, and cigarette smoke [2, 3]. Pyrolysis has often been shown to occur in oxygen deficient environments inside a burning cigarette. Temperatures typically range between 700 and 920°C, but occasional microenvironments can reach up to 1200°C [4]. Previous studies have found the formation of fullerene via pyrolysis of PAHs to occur in the 1000-1100°C range [1, 5]. In this work, we demonstrate fullerene production via pyrolysis of high-tar cigarette tobacco.

Concern over the potential environmental impact of fullerenes has risen sharply in recent years. Although pristine C_{60} has been considered to show minimal cytotoxicity to rat lungs and microbial communities, functionalized C_{60} has been found to show some level of cytotoxic effects [6, 7]. Fullerene water suspensions have been demonstrated to show pronounced cytotoxic effects when exposed to *E. coli*, *P. aeruginosa*, and *B. subtilis* [8, 9]. Additionally, fullerene exposure to ozone can also result in increased levels of toxicity. Ozone will add to a fullerene 6,6-double bond to form a 1,2,3-trioxolane which spontaneously converts to the fullerene epoxide, $C_{60}O$, producing singlet oxygen, a reactive oxygen species known for lipid peroxidation and membrane degradation [10]. Thus, inhalation of fullerene and exposure to even minimal amounts of ozone could lead to compromised membrane integrity in human lungs.

Therefore, considering the potential environmental impacts of C_{60}, our study sought to shed light on a (potentially) prevalent but previously unknown source of fullerenes.

Experimental Procedure:

Six samples of domestic cigarette tobacco and a control of untreated whole leaf Burley tobacco were pyrolyzed at various temperature maximums over a range of pressure profiles using a Thermcraft Protégé split tube furnace. Trials were performed under 100% argon flow with linear flow rates between 0.242 and 2.55 liters per minute. Smoke particulates were collected using PTFE 0.2 μm particulate filters and soluble ash and particulates were extracted into toluene using a Soxhlet apparatus. Two ash samples were also produced using custom-made smoking machines and extracted using the Soxhlet apparatus. Analysis on all samples was performed using a MALDI-TOF mass spectrometer.

Results and Conclusions:

MALDI-TOF analysis is believed to indicate fullerene content in the majority of ash samples. Seven of the nine samples displayed a possible C_{60} m/z (mass-to-charge ratio) peak of 720 and/or C_{70} m/z peak of 840. The remaining two samples displayed peaks that could correspond to hydroxyl and epoxy group additions to C_{60} or C_{70}. Of particular interest was evidence of C_{70}, but no clear amount of C_{60}, in M1, a sample run under high pressure and temperature. The most abundant amount of C_{60} appeared in M100-8, a sample run at lower temperature under near atmospheric pressure. Sample conditions are shown in Table 1. Overall, the spectral data provided compelling evidence for the formation of the C_{60} and C_{70} fullerenes during cigarette smoking events.

Based upon these results, we make the following recommendations to the scientific community: 1) Cigarettes should be viewed as potential sources of fullerene

environmental exposure, 2) Increased effort should be given to proper cigarette containment and ash disposal until the environmental effects of fullerenes are more fully understood, 3) Further research should be conducted in this area. Ultimately, the evidence shown in this work should be used to promote healthier and safer environmental conditions.

Future Work:

Further analysis is needed to confirm the presence of C_{60} and C_{70} in current samples. High performance liquid chromatography (HPLC) could be used to verify molecular UV-Vis spectra and retention times. In the future, additional high-carbon pyrolysis events should be investigated as potential fullerene sources. Cigar smoking is a natural candidate for such studies, as are forest fires and lean hydrocarbon fuel combustion.

Acknowledgements:

I would like to thank my Principal Investigator, Dr. John Fortner, for all his help, LeafOnly, LLC., for their generous donation of whole leaf tobacco, and the Pulmonary Mouse Genetic and Smoking Core for the use of their smoking machines. Credit and thanks to Dr. Fong-Fu Hsu for the use of the MALDI-TOF mass spectrometer, and particular thanks to Michael Pride for his ever-willing assistance. This work was sponsored by the National Science Foundation and the National Nanotechnology Infrastructure Network Research Experience for Undergraduates Program. Especial thanks to program coordinators Dee Stewart and Nathan Reed, and to all the NNIN staff who made this wonderful opportunity possible.

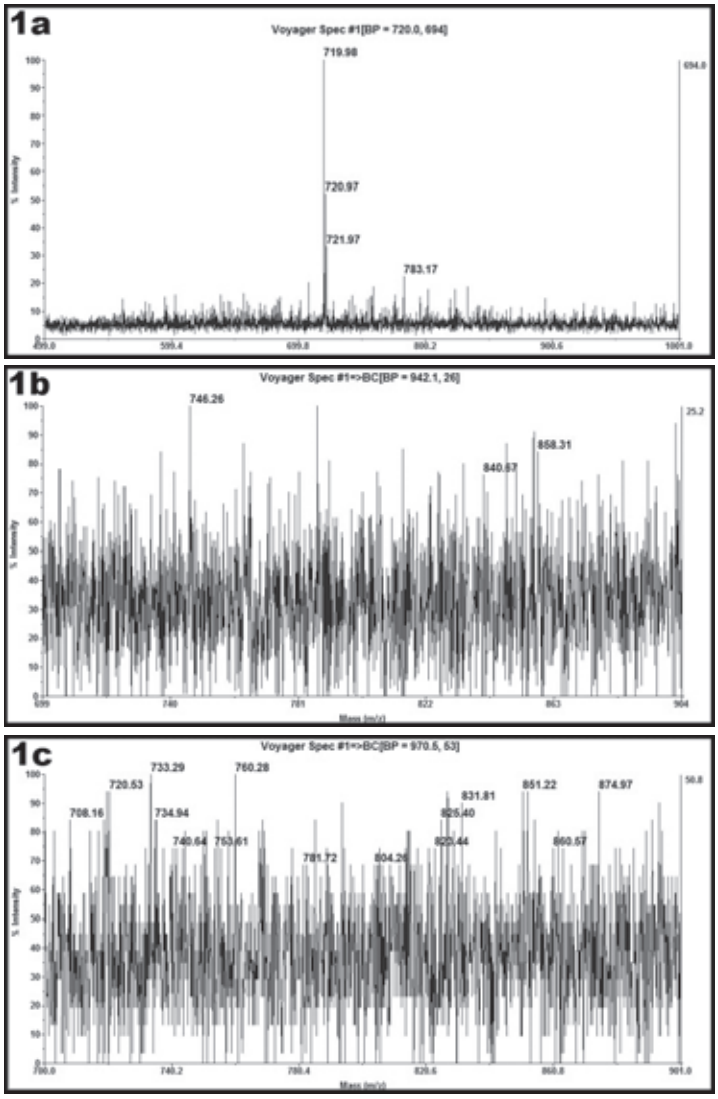

Figure 1: MALDI-TOF mass spectrum of samples a) M100-8, b) M1, and c) SM.

References:

[1] Taylor, Roger. Nature 366.6457 (1993): p.728-31.

[2] Alexeeff, G. Chronic Toxicity Summary Naphthalene. Environmental Health Hazard Assessment, http://oehha.ca.gov/air/chronic_rels/pdf/91203.pdf

[3] Ding, Yan S. Environmental Science and Technology 39.2: 471-78. (2005).

[4] Egerton, Alfred, K. Gugan, and F.j. Weinberg. Combustion and Flame 7: 63-78. (1963)

[5] Scott, Lawrence T. Science 295.5559: 1500-503. (2002).

[6] Baker, G. Toxicological Sciences 101.1: 122-31. (2007).

[7] Nyberg, Leila. Environmental Science and Technology 42.6: 1938-943. (2008).

[8] Kang, Seoktae. Environmental Science and Technology 43.7: 2648-653. (2009).

[9] Lyon, Delina Y. Environmental Science and Technology 40.14: 4360-366. (2006).

[10] Anachkov, Metodi P. Fullerenes, Nanotubes and Carbon Nanostructures11.2: 95-103. (2003).

Sample ID	Temperature Set-point (°C)	Initial Tube Pressure (torr)	Result
M1	1200	~2100 (~40psi)	Possible C70
M5	1200	608	C60
C6	1200	622	C60
M7	1200	747	Possible C70
M100-8	800	735	Large C60
C9	800	684	C60
Control	800	487	No Fullerene
SM*	Natural	Natural	No Fullerene
SC*	Natural	Natural	C60

Table 1: Summary of sample conditions and results.

Investigation of Molecular Structures for Soft Matters with Mechanoresponsive Colors

Kelly Suralik

Chemistry, Middlebury College

NNIN iREU Site: National Institute for Materials Science (NIMS), Tsukuba, Ibaraki, Japan

NNIN iREU Principal Investigator and Mentor: Dr. Kentaro Tashiro, Reticular Materials Group, International Center for Materials Nanoarchitectonics, National Institute for Materials Science

Contact: ksuralik@middlebury.edu, tashiro.kentaro@nims.go.jp

Abstract:

Materials with mechnoresponses are a new discipline in organic soft matter synthesis. One mechanoresponse, thixotropy, is the tendency of a material to become less viscous upon the addition of mechanical stress such as shaking. Separately in other gels, a visible color change during the gel-to-solution transition has been observed. While gels with either thixotropic or color-change qualities have been reported, the molecular structure of a thixotropic gel with mechanoresponsive colors has not yet been confirmed. In this work, we investigate molecular structures of gels. Synthesized platinum-terpyridine (Pt-terpy) complexes bearing an amino acid moiety were manipulated by changing solvent, counter anion and molecular structure. Pt-terpy gels and corresponding solution samples were analyzed through stable-by-inversion tests and emission spectroscopy. A thixotropic Pt-terpy gel without (fluoro-9-yl)methoxylcarbonyl (Fmoc) moiety exhibited a 648 nm emission peak, which indicated the presence of Pt-Pt interactions. Thixotropic gels that display mechanoresponsive colors may be applicable as oscillation sensors for buildings and earthquakes.

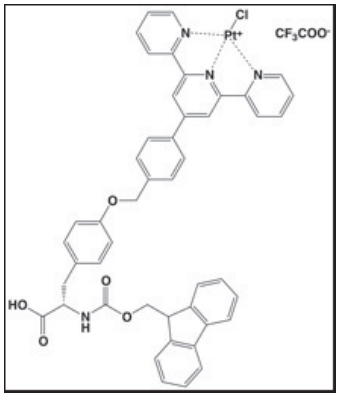

Scheme 1: Molecular structure of Pt-terpy thixotropic gel.

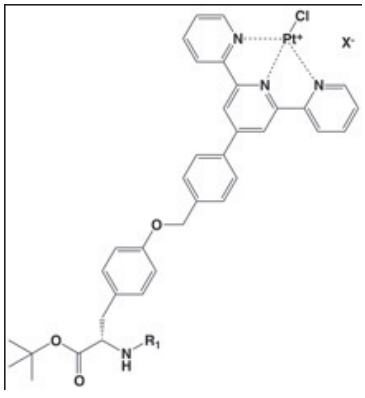

Scheme 2: Basic molecular structure for synthesized Pt-terpy complex analogs.

Introduction:

Polymers with mechanoresponsive colors display a change in color when stretched due to the presence of mechanically sensitive chemical groups in the polymer linkages [1]. However, other soft matters may be able to exhibit responses to mechanical stimuli. Thixotropy is the property of a material to become less viscous upon added shear stress. By shaking a thixotropic gel, the inherent network structure will break down, and the gel will undergo a phase change from gel to solution [2]. After standing, the material will return to its original state as the gel network reforms. In a separate phenomenon, some gels visibly change color during the gel-to-solution transition [3]. The color modification is related to the different metal interactions of the metal centers in the gel phase relative to the solution phase.

The National Institute for Materials Science International Center for Materials Nanoarchitectonics (NIMS MANA) Reticular Materials Group has previously synthesized a Pt-terpy thixotropic gel. The monomer for the thixotropic gel incorporates the Pt-terpy moiety and a functionalized tyrosine, shown in Scheme 1. The hydrogen bonding between the amino acid units are thought to cause the gelation capabilities of this complex. In addition, Pt-terpy possesses many spectral properties; specifically, emission at approximately 650 nm indicates Pt-Pt interactions [4]. However, the previously synthesized Pt-terpy thixotropic gel showed no absorption or emission that indicated the presence of Pt-Pt interactions.

A gel that exhibits both properties of thixotropy and color change upon phase transition has yet to be reported. In this study, we employed traditional organic synthesis procedures to manipulate the Pt-terpy complex structure in order to create a thixotropic gel with mechanoresponsive colors.

Experimental Procedure:

A series of Pt-terpy complexes of analogous forms were synthesized and tested for their gelation potential and color change ability. The basic structure is shown in Scheme 2. Counter anion salts in 10x molar excess were dissolved in Pt-terpy solutions for anion exchange. Alteration to the

original Pt-terpy complex was accomplished primarily through the metalation of Pt to a functionalized multidentate ligand followed by deprotection of Fmoc. Matrix-assisted laser desorption/ionizaton time-of-flight mass spectrometry (MALDI-TOF MS) was completed to ensure successful synthesis.

For gelation, the Pt-terpy complex was completely dissolved in solvent. Water was added to the solution to trigger gelation, followed by mixing of the reaction vial and standing. The presence of gel qualities was analyzed through the stable-by-inversion test.

Emission spectroscopy was employed on gel and solution samples of the synthesized Pt-terpy forms. Absorption spectroscopy was used to determine the necessary wavelength of excitation for emission measurements. Emission peaks were examined to determine the presence of Pt-Pt interactions.

Results and Conclusions:

The Pt-terpy complexes showed limited solubility in the water-miscible solvents (i.e. MeOH, CH_3CN), and dimethyl sulfoxide was selected as the best solvent for the water-triggered gelation protocol. Pt-terpy complexes with a trifluoroacetate (CF_3COO^-) counter anion increased the solubility of the complexes and formed gels. The Pt-terpy complex must be reasonably soluble in the solvent in order for the gelation test to be valid. The Pt-terpy complex with X = CF_3COO^- and R_1 = H was successfully synthesized (Scheme 2), and a thixotropic gel formed. Comparison of emission spectra between gel and solution samples of Pt-terpy complex (X = CF_3COO^-, R_1 = H) showed that only the gel state emitted at 648 nm, as seen in Figure 1. Comparison of emission spectra between complexes where R_1 = H or Fmoc demonstrated that only Fmoc deprotected Pt-terpy complexes emitted at 650 nm, as seen in Figure 2. It is hypothesized that deprotection of Fmoc reduced π-stacking and emphasized interaction between metal centers. Therefore, we synthesized a Pt-terpy thixotropy gel that contained Pt-Pt interactions.

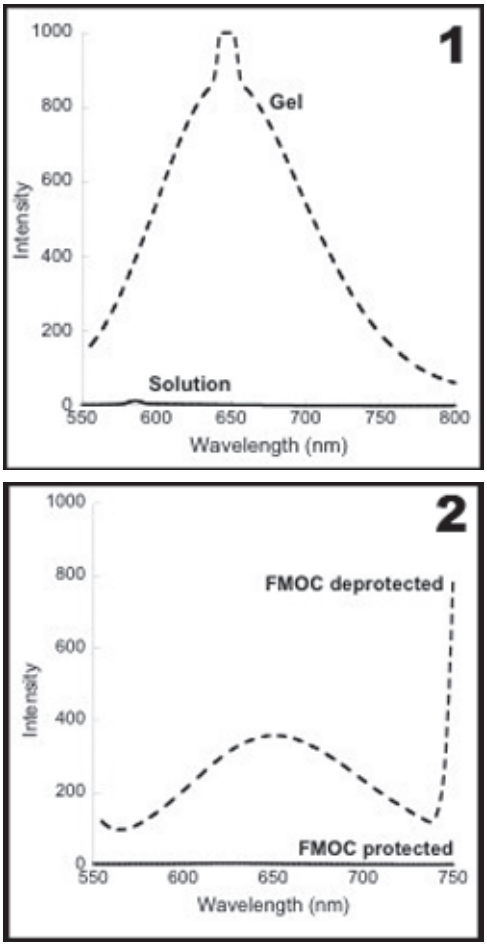

Figure 1, top: Emission spectra of [$^tBuO_2C$-Pt-NH_2][Cl][CF_3COO] gel and solution in DMSO/H_2O.

Figure 2, bottom: Emission spectra of [$^tBuO_2C$-Pt-NH_2][Cl][CF_3COO] and [$^tBuO_2C$-Pt-NHFmoc][Cl][CF_3COO] gels in DMSO/H_2O.

Future Work:

Future work will analyze the gel characteristics and emission spectral properties of a Pt-terpy complex capped with a phenylacetylene ligand. It is thought that the presence of the phenylacetylene ligand will emphasize Pt-Pt interactions through π-orbital stacking of the ligand near the metal center. Later studies will synthetically alter the Pt-terpy structure further in order to achieve mechanoresponsive colors.

Acknowledgements:

I extend sincere gratitude to Dr. Kentaro Tashiro and the Reticular Materials Group for their constant support. I thank NIMS, MANA, the NNIN Japan iREU interns, Dr. Lynn Rathbun, Dr. Nancy Healy, and Dr. James Marti. I would also like to thank Dr. Michael Deal for all of his encouragement. I acknowledge the National Nanotechnology Infrastructure Network International Research Experience for Undergraduates (NNIN iREU) Program and the National Science Foundation for financial support.

References:

[1] Davies, et al., Nature.2009,459, 68-72.

[2] Hoshizawa, et al., Chem. Lett. 2011,40, 1143-1145.

[3] Yuen, et al., Angew. Chem. Int. Ed. 2008,47, 9895-9899.

[4] Wong and Yam, Acc. Chem. Res. 2011,44, 424-434.

Effects of Membrane Surface Modification on Calcium Carbonate Fouling and Membrane Efficiency for Desalination

Whitney Wong

Biomedical Engineering, University of Texas at Austin

NNIN REU Site: Nano Research Facility, Washington University in St. Louis, St. Louis, MO
NNIN REU Principal Investigator: Dr. Young-Shin Jun, Department of Energy, Environmental and Chemical Engineering (EECE), Washington University in St. Louis
NNIN REU Mentor: Jessica Ray, EECE, Washington University in St. Louis
Contact: whitney.wong@utexas.edu, ysjun@seas.wustl.edu, jessica.ray@go.wustl.edu

Introduction:

Desalination can be used as a means to replenish freshwater supplies of communities with growing population needs. Reverse osmosis (RO) is a pressure-driven process that requires a semi-permeable membrane to selectively remove salts and other particulate matter from brackish water or seawater. Common RO membranes are thin-film composites (TFCs), which are composed of a thin polyamide layer supported by a porous polysulfone layer. Although membrane desalination is an efficient method, a persistent problem is that the membrane is highly susceptible to fouling—accumulation of particles onto the membrane surface over time that can clog or otherwise compromise the efficiency or performance of the membrane [1]. The main cause of fouling appears to be a hydrophobic interaction between the membrane surface and the solutes in the water [2]. In our approach, we grafted polyethylene glycol (PEG), a hydrophilic monomer, to help disrupt hydrophobic interactions with calcium carbonate ($CaCO_3$), a common hydrophobic fouling agent (Figure 1). After membrane characterization, we analyzed the interaction between $CaCO_3$ and the membrane surface.

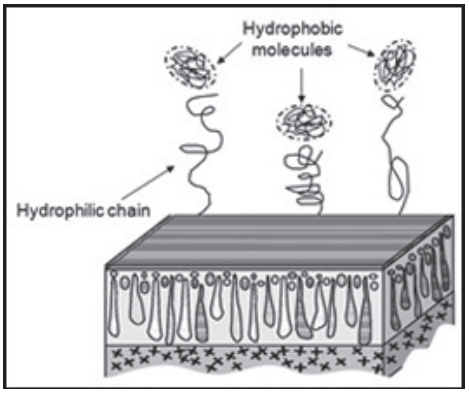

Figure 1: Experimental approach. Graft PEG to membrane surface to help reduce fouling of hydrophobic solutes [3].

Experimental Procedures:

Monomer Grafting. Commercially available BW30 TFC membranes were purchased from Dow-Filmtec in flat sheet form. Grafting materials purchased from Sigma-Aldrich included potassium disulfite (PD) and potassium persulfate (PP) to initiate the reaction, polyethylene glycol (PEG) as the hydrophilic monomer, and ethyleneglycol dimethacrylate (EGDMA) as the crosslinker. Various concentrations and grafting times were tested. The final conditions chosen were a graft time of one hour with a solution that consisted of 0.1 M PEG, 0.01 M EGDMA, and a 0.025 M equimolar PP and PD solution.

Contact Angle. To determine the wettability of the membrane, we measured contact angles of samples with and without surface modification. Twenty microliters of de-ionized (DI) water was pipetted onto the membrane surface, where images were then captured using a Motic digital microscope and the Motic Image Plus 2.0 software.

$CaCO_3$ Nucleation and Salinity Testing. Various concentrations of sodium bicarbonate ($NaHCO_3$) and calcium chloride dihydrite ($CaCl_2$) were used to form $CaCO_3$, which could be deposited onto the membrane surface. To mimic brackish water conditions, we replaced double-filtered water in the original solution with a background solution of sodium chloride (NaCl). Concentrations of 0.1, 0.5, and 1 M NaCl were added to observe the effect of increasing NaCl on $CaCO_3$ formation.

Because the $CaCO_3$ saturation index (SI) changes with ionic strength, the Geochemist's Workbench software was used to calculate the adjusted $CaCl_2$ and $NaHCO_3$ concentrations to maintain an SI of 2.16 for calcite formation for all experiments.

Thus, a final solution with concentrations of 0.025 M $NaHCO_3$ and 0.025 M $CaCl_2$ was used.

Results and Discussion:

Characterization of the membrane before and after grafting included scanning electron microscopy (SEM) and measuring contact angles. In order to see whether grafting was successful, contact angle measurements were determined to observe whether grafting made the membrane more hydrophilic. The best concentration, 0.1 M PEG for one hour, was chosen because it had a smaller contact angle than the unmodified membrane.

SEM proved to be a powerful tool for analyzing both the unmodified and grafted membranes after $CaCO_3$ was deposited onto the surface. As the NaCl concentration increased, there was a definite increase in $CaCO_3$ nucleation for both the unmodified and grafted membranes. An increase in nucleation as ionic strength increases has been reported in literature [4]. There was also a distinct decrease in the amount of nucleation between the unmodified and grafted membranes at each respective concentration of NaCl. For example, this can be seen in Figures 2 and 3.

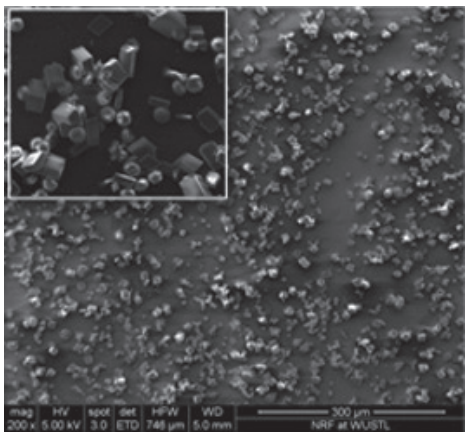

Figure 2: Unmodified membrane with $CaCO_3$ nucleation and a background solution of 0.5 M NaCl. Inset in the upper left corner is magnified with a scale of 40 µm.

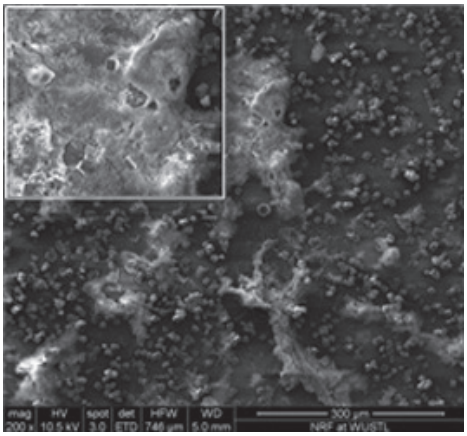

Figure 3: PEG-grafted membrane with $CaCO_3$ nucleation and a background solution of 0.5 M NaCl. There is less nucleation around and on dense areas of PEG. Inset in upper left corner is magnified with a scale of 50 µm.

A final observed trend was a difference in $CaCO_3$ morphologies. In the unmodified membrane, amorphous $CaCO_3$ (spherical), calcite (rhombohedral), and aragonite (fibrous-shaped) were identified. While in the grafted membrane, mostly calcite was observed. This could be due to the differences in binding sites after grafting with PEG.

Conclusions and Future Work:

In this project, PEG was successfully grafted onto the TFC membrane surface. From the SEM images of both the unmodified and grafted membranes, there was clearly a decrease in the degree of $CaCO_3$ nucleation as the surface became more hydrophilic. This was what was expected when a hydrophilic component was added to the membrane. After analyzing the interaction between the membranes and the $CaCO_3$ particles, it was determined that hydrophilic/hydrophobic interactions govern nucleation.

In the future, a working laboratory-scale RO system is desired to test grafted membrane efficiency in salt rejection. There are implications for this grafting procedure to be a viable modification that could help to reduce water pretreatment costs, extend the lifetime of TFC membranes, and improve the overall membrane desalination process. Thus, it is extremely important to test and compare the efficiency of the unmodified and grafted membranes.

Acknowledgements:

Thank you to Dr. Young-Shin Jun, Jessica Ray, and everyone at the Environmental Nanochemistry Lab for their guidance and support. I would also like to give thanks to the Nano Research Facility, the National Nanotechnology Infrastructure Network Research Experience for Undergraduates (NNIN REU) Program, and the National Science Foundation for giving me this opportunity and an unforgettable experience.

References:

[1] Freger, et al.; Membrane Science, 209, 283-292 (2002).

[2] Koo, et al.; "Fouling resistant reverse osmosis membranes"; 1-10 (2003).

[3] Kang, et al.; Polymer, 48, 1165-1170 (2007).

[4] Boerlage, S.; "Scaling and particulate fouling in membrane filtration systems"; Dissertation, Swets and Zeitlinger Publishers, 208 (2001).